The Planetary Science Journal, 2:156 (9pp), 2021 August https://doi.org/10.3847/PSJ/ac134f

A Case for a Small to Negligible Influence of Dust Charging on the Ionization Balance in the Coma of Comet 67P

E. Vigren[1], A. I. Eriksson[1], F. L. Johansson[1], R. Marschall[2], M. Morooka[1], and M. Rubin[3]
[1] Swedish Institute of Space Physics, Uppsala, Sweden; erik.vigren@irfu.se
[2] Department of Space Studies, Southwest Research Institute, Boulder, CO, US
[3] Physikalisches Institut, University of Bern, CH-3012 Bern, Switzerland
Received 2021 April 1; revised 2021 July 9; accepted 2021 July 10; published 2021 August 10

Abstract

A recent work aided by Rosetta in situ measurements set constraints on the dust-to-gas mass emission ratio and the size distribution of dust escaping the nucleus of comet 67P/Churyumov–Gerasimenko near perihelion. Here we use this information along with other observables/parameters as input into an analytical model aimed at estimating the number density of electrons attached to dust particles near the position of Rosetta. These theoretical estimates are compared to in situ measurements of the degree of ionization. The comparison proposes that Rosetta, while near perihelion, was typically not in electron-depleted regions of the inner coma of 67P. Our work suggests a typical level of electron depletion probably below 10% and possibly below 1%. In line with previous studies, we find, again with certain assumptions and other observables/parameters as input, that the observed negative spacecraft charging to a few tens of volts does not significantly impact the detection of charged dust grains, with a possible exception for grains with radii less than ∼10 nm.

Unified Astronomy Thesaurus concepts: Comets (280)

1. Introduction

Regions of ionospheres where the number density of free electrons is significantly lower than the number density of positively charged ions are referred to as electron depleted. It has since long been known that the D region of Earth's ionosphere is electron depleted (e.g., Larsen et al. 1972) due to, e.g., the formation of negative ions via three-body reactions. Research over the last decade has shown that electron depletion need not be limited to such high-pressure regions where three-body reactions are believed to be efficient. The Cassini mission revealed electron depletion in the plume of Enceladus (Morooka et al. 2011), in Titan's deep ionosphere (Shebanits et al. 2013) as well as in the ionosphere of Saturn (Morooka et al. 2019). In the case of Enceladus, the depletion is attributed mainly to attachment to icy grains, down to nanometer scale, emanating from geysers on the southern hemisphere. In Titan's ionosphere, photochemically produced complex organic molecules, of ∼nanometer size, act as sites for electron attachment (e.g., Coates et al. 2007; Lavvas et al. 2013).

Cometary comae almost intuitively seem plausible regions for electron depletion. Active comets are known to emit comparable amounts of dust as gas in terms of mass (e.g., Snodgrass et al. 2013). It is mainly dust (reflecting sunlight) that sometimes makes comets visible to the naked eye. To the best of our knowledge, no study based on in situ measurements in the inner coma of comet 67P/Churyumov–Gerasimenko (henceforth 67P) has addressed the question of whether the Rosetta spacecraft ever resided in strongly electron-depleted regions. Our interest in this question is strongly tied to the above-mentioned, and rather recent, discoveries of electron-depleted plasmas elsewhere in the solar system, and we seek to explore the question of whether the more classical quasi-neutrality condition "$n_e \approx n_i$", often assumed in ionospheric modeling efforts, ever holds in regions with putative electron attachment sites (icy particles, complex organics, and dust grains). Adding to our interest in the raised question is that grain charging has been raised as a plausible contributing reason as to why cometary ionospheric models assuming ions to move radially outwards at the same speed as the neutral gas perform worse in reproducing observed electron number densities near perihelion than at lower activity (e.g., Vigren et al. 2019 and references therein).

The confirmation of electron number densities falling short of the positive ion number densities ($n_e \ll n_i$) in regions probed by Cassini was possible thanks largely to the high spacecraft velocity (several to several tens km s^{-1}). In particular, extracting ion number densities from Langmuir probe sweep analysis is simplified when it safely can be assumed that the ion velocity relative to the spacecraft is dictated mainly by the spacecraft velocity itself (e.g., Morooka et al. 2011). In addition, with a high spacecraft velocity, negative ions could be observed clearly with the Electron Spectrometer (CAPS/ELS; e.g., Coates et al. 2007; Hill et al. 2012). While carrying similar instrumentation, Rosetta moved at a walking pace (∼a m s^{-1}) around the nucleus of 67P, making it difficult to confirm or rule out non-negligible electron depletion by similar means.

Adapting the grain charging formalism of Draine & Sutin (1987) and several simplifying assumptions, Vigren et al. (2015) modeled (before the Rosetta arrival) grain charging in the coma of 67P. From their results and sensitivity tests, they proposed that prominent electron depletion out to a few hundreds of kilometers from the nucleus requires a ubiquitous presence of grains in the nanoscale regime. For instance, with a dust-to-gas emission ratio of unity and with all grains (artificially) being in the form of spheres with 100 nm radius there would, according to their model runs, be virtually no electron depletion at all at distances >10 km from the nucleus. On the contrary, with a few percent of the mass being in the form of ∼2 nm grains an electron depletion exceeding 50%

could prevail to distances exceeding 100 km. There are reasons to revisit the model of Vigren et al. (2015) in light of subsequent results from Rosetta. In particular, sensitivity tests should be carried out for much higher electron temperatures than considered in the original work. In the present work we consider, however, a completely different grain charging model, which is analytical in nature.

The outline of the paper is as follows. In Section 2 we present the theoretical framework for assessing the number density of electrons on dust particles, $n_{e,\mathrm{dust}}$. Simplifying assumptions, like that of radially moving gas and dust, allow us to derive an analytical expression (Equation (3)) whereby $n_{e,\mathrm{dust}}$ can be calculated from a closed-form expression, although one including as many as 11 "tunable" parameters. In Section 3 we discuss the parameter space and seek to justify our selection of default values. We make use of recent results from Marschall et al. (2020) to constrain some of the dust parameters of the analytical model, including the exponent of the power-law size distribution, the size dependence of the dust grain velocity, and the total dust-to-gas mass emission ratio near perihelion. In Section 4 we first (Section 4.1) compare theorized $n_{e,\mathrm{dust}}/n_N$ ratios (n_N denoting the number density of neutral molecules) with observed n_e/n_N ratios near perihelion. The comparison, in combination with the discussions of the parameter space in Section 3, speaks in favor of a typically much less dramatic level of electron depletion in the comet environment (at the position of Rosetta) than in the plume of Enceladus (as "seen" by Cassini). In Section 4.2 we briefly reflect on a question raised earlier (e.g., Fulle et al. 2015): Did the negative spacecraft potential of Rosetta (typically −10 to −15V or even more negative; Odelstad et al. 2017) act in a size-discriminating fashion, prohibiting parts of the population of negatively charged grains from reaching onboard instrumentation? In short—we believe not, with the possible exception of grains as small as 10 nm and smaller, for which there anyway is little observational evidence besides occasional detections by the Ion Electron Sensor (IES) of charged nanograins (of both polarities) moving roughly anti-sunward (Burch et al. 2015; Llera et al. 2020). A summary with concluding remarks is given in Section 5.

2. Analytical Model

We assume an ensemble of radially expanding dust particles that quickly reach their terminal velocity as seen in simulations by e.g., Davidsson et al. (2010) and Tenishev et al. (2011). The number flux of dust grains in the size range $[r, r+dr]$ is taken to be $c_1 r^{-\alpha} dr$, where c_1 (units of $\mathrm{m}^{\alpha-3}\mathrm{s}^{-1}$) and α are positive constants and r is the grain radius. We restrict $r_{\min} < r < r_{\max}$. For a radially expanding water-dominated gas coma, the gas mass flux at the location of Rosetta is given by $n_N m_w u_{\mathrm{gas}}$, where n_N is the number density of neutral molecules, m_w is the mass of a water molecule, and u_{gas} is the gas expansion velocity. Introducing χ as the dust-to-gas mass emission ratio we realize that

$$c_1 \int_{r_{\min}}^{r_{\max}} \frac{4\pi r^3}{3} \rho r^{-\alpha} dr = \chi n_N m_w u_{\mathrm{gas}}, \quad (1)$$

Table 1
Default Parameters Used when Calculating $n_{e,\mathrm{Dust}}$ from Equation (3) and n_n

Parameter	Values	Comment
$r_{\min}$	10 nm (Type 1), 100 nm (Type 2)	See Section 3.2
$r_{\max}$	0.1 m	See Section 3.2
α	3.6 (Type A), 3.7 (Type B), 3.8 (Type C)	See Section 3.3
χ	0.73	See Section 3.3
c_2	0.234 9 [$\mathrm{m}^{\beta+1}\mathrm{s}^{-1}$]	See Section 3.4
β	0.427 2	See Section 3.4
ρ	533 [$\mathrm{kg\ m}^{-3}$]	See Section 3.4
U_D	−10 [V]	See Section 3.5
κ_e	2	See Section 3.5
u_{gas}	750 [$\mathrm{m\ s}^{-1}$]	See Section 3.5

Notes. The parameter set is split into six types: 1A, 1B, 1C, 2A, 2B, and 2C, depending on the values of the parameters $r_{\min}$ and α.

where ρ is the dust mass density and where we have assumed spherically shaped grains. From this follows that

$$c_1 = \frac{3(4-\alpha)\chi n_N m_w u_{\mathrm{gas}}}{4\pi\rho} \frac{1}{r_{\max}^{4-\alpha} - r_{\min}^{4-\alpha}}. \quad (2)$$

Next we assume that the (quickly reached) terminal velocity of individual grains has a size dependence of $u_D(r) = c_2 r^{-\beta}$, where c_2 (with units of $\mathrm{m}^{\beta+1}\mathrm{s}^{-1}$) and $\beta > 0$ are constants. This can be used to transform the number flux size distribution into a local number density size distribution $(c_1/c_2)r^{\beta-\alpha}$ at the position of Rosetta. We assume that any given dust particle is in charge equilibrium, carrying a charge Q_r given by the product of a size-independent potential U_D and a size-dependent capacitance $C(r) = 4\pi\varepsilon_0\kappa_e r$, where ε_0 is the permittivity of free space and κ_e is an appropriate (dimensionless) dielectric constant (e.g., Fulle et al. 2015). The total dust charge density due to charged dust grains is found by integrating Q_r over the dust number density size distribution. Dividing by the elementary charge, we arrive (using c_1 from Equation (2)) at the following expression for the local number density of electrons attached to dust:

$$n_{e,\mathrm{dust}} = \frac{3(4-\alpha)}{2+\beta-\alpha} \frac{u_{\mathrm{gas}} m_w}{c_2 \rho} \frac{\varepsilon_0}{q} \times \left(\frac{r_{max}^{2+\beta-\alpha} - r_{min}^{2+\beta-\alpha}}{r_{max}^{4-\alpha} - r_{min}^{4-\alpha}} \right) \chi \kappa_e U_D n_N. \quad (3)$$

This serves as the key equation of our work and is applicable for $\alpha \neq 4$ and $\alpha \neq 2+\beta$.

3. Parameter Space and Discussions Thereof

3.1. Initial Remarks

A quick glance on the right-hand side of Equation (3) reveals 11 parameters that in one way or another require determination or constraint-setting by in situ measurements, modeling/simulation efforts, and/or educated guesses. We note that our default parameter set (see Table 1) and subsequent comparisons are directly or indirectly based on/guided by measurements by a suite of Rosetta instruments including GIADA, OSIRIS, MIDAS, CONSERT, VIRTIS, ROSINA/COPS, MIRO, RSI, RPC/MIP, and RPC/LAP (the acronyms will be explained later). For several of our selected default parameters, there are conflicting "views" in the literature. We stress, and we will

stress again, that it is not our aim to pinpoint the level of electron depletion in the inner coma. Such a goal would be unrealistic considering the underlying (simplified) theoretical framework and the mere immensity of the involved parameter space. Rather, we make the soft case that it does seem, from the evidence and clues at hand, that Rosetta was typically not in strongly electron-depleted regions while orbiting 67P (at distances of a few hundred kilometers) near its perihelion passage in 2015 August. Our default parameter set is split into six subsets that we shall refer to as 1A, 1B, 1C, 2A, 2B, and 2C. Sets of type "1" and "2" consider a minimum dust size radius of 10 nm and 100 nm, respectively. Sets of type "A", "B," and "C" consider size distribution power-law exponents of −3.6, −3.7, and −3.8, respectively.

Among investigations into the dust size distribution and dust-to-gas mass emission ratios our work relies mostly on the recently published study of Marschall et al. (2020). They utilized a 3D Direct Simulation Monte Carlo (DSMC) gas dynamics code to simulate the inner gas coma of 67P while the dust coma was simulated by means of a 3D dust dynamics code including gas drag and the gravitational influence of the nucleus. The gas model was constrained by in situ measurements from the Rosetta Orbiter Spectrometer for Ion and Neutral Analysis/COmet Pressure Sensor (ROSINA/COPS; Balsiger et al. 2007) while the use of advanced dust scattering properties allowed synthetic images to be produced for comparisons with the dust coma brightness as measured by the Optical, Spectroscopic and Infrared Remote Imaging System (OSIRIS; Keller et al. 2007). The simulations (and associated comparisons) allowed properties of the dust coma to be constrained, as detailed further below. It is worthwhile mentioning that Marschall et al. (2020) present their obtained parameter values with asymmetric uncertainties, the range of which we do not take into consideration here because the individual best-fit values are intertwined and not fully independent. For instance, still reasonable solutions with steeper dust size distributions than adapted in this work come with larger minimum dust sizes to still be in line with the dust coma brightness measured by OSIRIS (see Table 5 in Marschall et al. 2020).

3.2. The Parameters r_{min} and r_{max} (Minimum and Maximum Dust Sizes)

For a fixed mass flux the calculated value of $n_{e,\mathrm{dust}}$ increases when reducing r_{min} and r_{max}, displaying a higher sensitivity to a reduction of r_{min} than to a change in r_{max}. That the lower end of the size range has a paramount impact on the calculated $n_{e,\mathrm{dust}}$ is in line with the qualitative results of Vigren et al. (2015) discussed briefly in Section 1. Let us first note that setting $r_{\mathrm{max}} \approx 10^{-1}$ m is justified by the work of Marschall et al. (2020), particularly in view of their Figure 9 showing the largest escaping dust size as a function of the gas production rate.

As very small particles (several tens of nm or smaller) are practically invisible to OSIRIS, Marschall et al. (2020) could not set a lower limit for the smallest dust size. Rather, they showed that the smallest dust size must be strictly smaller than 30 μm and purportedly smaller than ∼12 μm. We consider for the time being, and with the evidences at hand, $r_{\mathrm{min}} = 10$ nm (invoked in the Type 1 parameter sets) to indeed be a low estimate. First, high spatial resolution (down to 8 nm) imaging with the MIDAS Atomic Force Microscope on board Rosetta shows a micrometer-sized particle to contain subunits in the hundreds of nanometer range, which in turn comprise surface features/possible subunits with a log-normal size distribution, a mean diameter of ∼100 nm, and a minimum diameter of ∼50 nm (Mannel et al. 2019). If grains with radii <10 nm would be ubiquitous, then, considering the high spatial resolution of MIDAS, the near lack of clear features with diameters <50 nm seem challenging to explain. Güttler et al. (2019) consider particles with diameters of 50–500 nm as the smallest particles, possibly classified into what they refer to as a solid group, although for this discussion they refer primarily to the original work of Mannel et al. (2019), wherein the presented log-normal size distribution is based on high-resolution imaging of a single grain.

Reported detections of charged nanograins by the IES (Burch et al. 2007) have thus far focused mainly on ones with an anti-sunward motion (Burch et al. 2015; Llera et al. 2020). Their (occasional) presence possibly indicates a formation via fragmentation/erosion of larger grains at a distance from the nucleus and subsequent acceleration "back" by the solar radiation pressure and electromagnetic forces (Gombosi et al. 2015). It should also be noted that an electrostatic analyzer like the Rosetta IES is not an instrument designed for dust measurements, nor was IES calibrated for this purpose. While the interpretation by Burch el al. (2015) and Llera et al. (2020) of certain signatures in IES data as due to charged dust grains of very small size is very plausible, the deduction of detailed properties like grain size may still be subject to large uncertainties. For instance, without a detailed knowledge of the fate of a charged grain and its chance of fragmentation as it collides with the IES components, some of which are biased to high voltages, it could be difficult to distinguish in observations the instrument effects on the ultimate grain size from the actual grain size carried by the cometary plasma. It may be prudent to consider the IES constraints on dust size to be relatively weak. Johansson et al. (2017) proposed that an observed reduction, lasting months around perihelion, in the Langmuir Probe (LAP; Eriksson et al. 2007) photoelectron emission (relative to what would be expected from extrapolated unattenuated solar extreme ultraviolet spectra) could be caused by a far upstream (partial) fragmentation of cometary dust into subunits of sizes of a few tens of nanometer (compatible with the smallest features reported by Mannel et al. 2019). Fragmentation of a dust particle into many subunits contributes to enhanced attenuation simply because the total cross-sectional area increases. As the relative reduction in photoemission current displayed no dependence on the cometocentric distance of Rosetta (not even during an excursion), it was argued by Johansson et al. (2017) that a profound fragmentation/erosion probably did not commence in between the nucleus and the location of Rosetta, but only far upstream. Works based on data from ground-based observations of 67P include ones arguing for (e.g., Boehnhardt et al. 2016) and against (e.g., Moreno et al. 2017) grain fragmentation/erosion far away from the nucleus.

The use of $r_{\mathrm{min}} = 100$ nm in the Type 2 parameter settings is justified essentially by the lack of any evidence for an ambient and ubiquitous presence of much smaller particles. At least during outbursts near perihelion the presence of submicron particles (⩽100 nm) was confirmed from the analysis of Visible and Thermal Imaging Spectrometer (VIRTIS) high-resolution observations (Bockelée-Morvan et al. 2017).

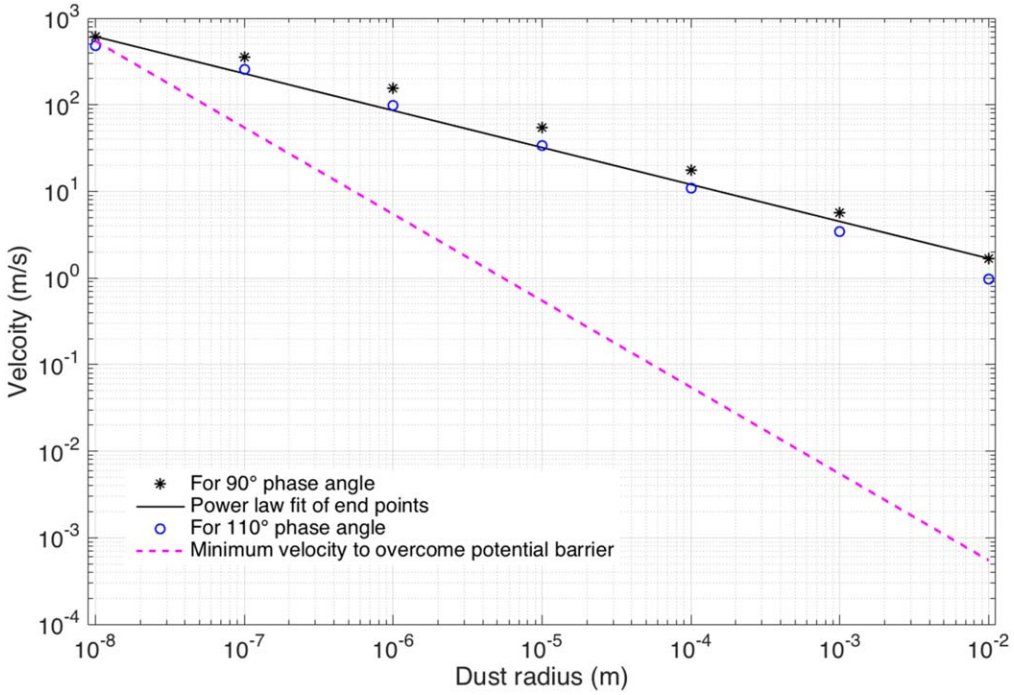

Figure 1. Dust velocity vs. size extracted from the numerical simulations of Marschall et al. (2020). The black asterisks (blue circles) are for a phase angle of 90° (110°). The black line connects the two extreme points via a power-law fit $u_d(r) = c_2 r^{-\beta}$ yielding $c_2 = 0.2349$ $m^{\beta+1}s^{-1}$ and $\beta = 0.4272$. The dashed magenta line corresponds to the minimum velocity needed for a grain of mass density 533 kg m^{-3} that has reached equilibrium charge to overcome the barrier associated with a spacecraft potential of −15 V (cf. Equation (9); $U_D = -10$ V; $\kappa_e = 2$).

3.3. The Parameters α and χ (Power Index and Dust-to-gas Mass Emission Ratio)

The face values for α and χ suggested from the work of Marschall et al. (2020) are 3.7 and 0.73, respectively. Both of the parameters are such that an increased value yields an increase in the calculated value of $n_{e,\mathrm{dust}}$. While adapting $\chi = 0.73$ as a default parameter value, we consider α values of 3.6, 3.7 and 3.8 in calculations of Types A, B, and C, respectively. The quoted dust-to-gas mass emission ratio of $\chi = 0.73$ is almost an order-of-magnitude lower than suggested by Moreno et al. (2017) and Ott et al. (2017). In support of their lower established ratio, Marschall et al. (2020) note that the earlier estimates are inconsistent with the total mass loss inferred from detailed nucleus mass determinations, pre- and post-perihelion, by the Radio Science Investigation (RSI; Pätzold et al. 2019).

Our adapted value of α (from Marschall et al. 2020) is consistent with near-perihelion measurements by the Grain Impact Analyser and Dust Accumulator (GIADA) and the COmetary Secondary Ion Mass Analyser (COSIMA) suggesting, respectively, power-law exponents of −3.7 (Fulle et al. 2016) and -3.8 ± 0.9 (Merouane et al. 2017). It should be mentioned that the inferred power-law exponents evolved over the Rosetta mission (e.g., Fulle et al. 2016; Merouane et al. 2017). For further comparison with power-law indices reported in the literature, one should also pay attention to whether authors refer to a flux distribution, a number density distribution, or cumulative versions thereof. Finally, a single exponent may not adequately describe the size distribution over the full range of dust sizes (e.g., Moreno et al. 2017). Such an assumption is, however, necessary for our simple analytical approach. Qualitatively speaking, introducing anywhere a steeper subpart (less steep subpart) would tend to enhance (decrease) the calculated value of $n_{e,\mathrm{dust}}$.

3.4. The Parameters c_2, β, ρ, and u_{gas} (Velocity Parameters and Dust Mass Density)

The velocity of dust particles as a function of size and phase angle is an output of the simulations made in Marschall et al. (2020). The phase angle (solar zenith angle) over the considered time period (∼half a month pre-perihelion to one month after perihelion) was stable near 90° up until about a week post-perihelion (terminator orbit). Thereafter the phase angle dropped over the course of roughly a week to be stable around 70° for an additional few days before gradually increasing. Only for the last week of the considered time interval did the phase angle exceed 90°, peaking at ∼120° (see Figure 8 of Hansen et al. 2016). We consider here for simplicity a phase angle of 90° and results (see Figure 1, black asterisks) obtained from simulations adapted to high-activity conditions a few weeks post-perihelion assuming grains of mass density $\rho = 533$ kg m^{-3} (set similar to to the bulk density of the nucleus; Pätzold et al. 2016). The use of $c_2 = 0.2349$ $m^{\beta+1}s^{-1}$ and $\beta = 0.4272$ gives velocities that agree with the simulations results for dust radii of 10 nm and 1 cm, while for radii strictly within this size range, the velocities found via $u_D(r) = c_2 r^{-\beta}$ fall somewhat short of those found from the simulations (reasonably fitting simulation results for a phase angle of 110°; see blue circles in Figure 1).

Using too small velocities implies the risk of overestimating $n_{e,\mathrm{dust}}$. However, the effect is not dramatic, and a simple power-law relation is desirable (even necessary) for our simple analytical framework. Moreover, crudely speaking, the possibly underestimated grain velocities adapted here give some freedom for adjusting upwards the adapted value of the mean

density of the dust grains, ρ. Marschall et al. (2020) use the same assumption of $\rho = 533\,\mathrm{kg\,m^{-3}}$ in most of their simulations, noticing that the exact relationship of the density as a function of dust size is unknown. Compact grains have been reported from GIADA measurements to have densities in the range 800–3000 $\mathrm{kg\,m^{-3}}$ (Rotundi et al. 2015). On the other hand, for fluffy grains collected with COSIMA, Hornung et al. (2016) reported mass densities lower than for the nucleus. In this work, similar to Marschall et al. (2020), we assume dust and nucleus densities to be equal and therefore within the range bracketed by fluffy and compact grains. We note that $n_{e,\mathrm{dust}}$ scales with χ/ρ according to Equation (3), and we mentioned in Section 3.3 that the dust-to-gas mass emission ratio $\chi = 0.73$ from Marschall et al. (2020) is lower than suggested by Moreno et al. (2017) and Ott et al. (2017). Clearly, scaling up χ and ρ by similar factors has no influence on the calculated $n_{e,\mathrm{dust}}$ when leaving all other parameters of Equation (3) fixed.

Finally, for a phase angle of 90° and near perihelion (heliocentric distance of ∼1.25 au), the default gas expansion speed is, based on the work of Hansen et al. (2016), set to $u_{gas} = 750\,\mathrm{m\,s^{-1}}$. This is in reasonable agreement with velocities inferred from measurements by the Microwave Instrument for the Rosetta Orbiter (MIRO; see Figure 5 in Biver et al. 2019) and ∼20% higher than the terminal velocity of the smallest dust grains considered in this work.

3.5. The Parameters κ_e and U_D (Dielectric Constant and Grain Potential)

The relative permittivity of 67P dust particles is discussed/constrained by Herique et al. (2016) based on analysis of CONSERT measurements (CONSERT is the acronym for Comet Nucleus Sounding Experiment by Radiowave Transmission). They conclude that $\kappa_e < 5.4$ with the upper limit corresponding to dense dust having no micro- or macro-porosity. The effect of lowering the assumed mass density can be seen in their Figure 6, and in fact, for mean densities as low as our default value ($533\,\mathrm{kg\,m^{-3}}$) the work of Herique et al. (2016) seemingly suggests values of κ_e below 2. The value of κ_e for individual dust particles in the coma is anticipated (e.g., Fulle et al. 2015) to be sensitive to the shape of the particles, with more compact spherical particles possessing lower values (closer to unity) than irregular, fluffier ones. We set as a default value $\kappa_e = 2$.

For grains in a water ion plasma, Notni & Tiersch (1987) predict a potential of $U_D \approx -3.66\,T_{\mathrm{eV}}$ with T_{eV} the electron temperature in eV. Measurements by the dual LAP and the Mutual Impedance Probe (MIP) revealed the plasma around 67P to typically be composed of a warm and a cold population with temperatures of ∼5 eV and ∼0.1 eV, respectively (Eriksson et al. 2017; Engelhardt et al. 2018; Odelstad et al. 2018; Gilet et al. 2020). We set as a default value $U_D = -10$ V, corresponding in the above formalism to a mean electron temperature of ∼2.7 eV, which is realized by roughly equal fractions of cold and warm electrons. It is noted that the fraction of cold electrons at times accounted for as much as 60%–90% of the total electron population (Gilet et al. 2020). It should be mentioned that the use of this simple formalism for the grain potential comes with the risk of overestimating $n_{e,\mathrm{dust}}$, and in certain dusty plasmas even strongly so. For instance, photodetachment of electrons from grains contributes to driving the grain potential more positive and is implicitly ignored in the current setup as the process is not considered in the work of Notni & Tiersch (1987). Also, there are only a finite supply of electrons to soak up from the plasma and there may in cases simply not be enough electrons around for the typical grain potential to even approach values like $-3.66\,T_{\mathrm{eV}}$. In his review on dust charging in plasmas, Goree (1994) refers to this effect as "charge reduction at high dust densities." Readers are also referred to, e.g., Mendis & Horányi (2013) and Meyer-Vernet (2013) for in-depth descriptions of the physics and processes influencing dust charging. The point addressed is that Equation (3) in a formal sense targets an upper limit of $n_{e,\mathrm{dust}}$ as the underlying assumption that the grains have (or even can) reach equilibrium charge may not be valid. To clarify, however, when applying a parameter set to Equation (3), we cannot, due to uncertainties in input parameters, say that we by strict necessity calculate a lower value of $n_{e,\mathrm{dust}}$ than actually present.

Table 2
Calculated $n_{e,\mathrm{Dust}}/n_N$ Ratios for the Six Parameter Sets Considered (see Table 1 and Equation (3))

Type	$n_{e,\mathrm{Dust}}/n_N$	Type	$n_{e,\mathrm{Dust}}/n_N$
1A	8.96×10^{-7} [∼2%]	2A	6.03×10^{-8} [∼0.1%]
1B	3.12×10^{-6} [∼7%]	2B	1.68×10^{-7} [∼0.4%]
1C	9.99×10^{-6} [∼20%]	2C	4.34×10^{-7} [∼1.1%]

Note. A "typical" corresponding level of electron depletion is shown within brackets adapting Equation (8) and the median ($=4.06 \times 10^{-5}$) of the observed n_e/n_N ratio observed near perihelion.

4. Results and Discussions

4.1. Calculated $n_{e,dust}$ and Comparisons to Measured Number Densities of Free Electrons

The parameter set(s) of Table 1 allows via Equation (3) to directly compute the $n_{e,\mathrm{dust}}/n_N$ ratio. The resulting ratios for the six considered parameter sets are listed in Table 2 and illustrated also by horizontal lines in Figure 2(b). Comparisons with measured electron and neutral number densities allow us to tie these results to estimates of the level of electron depletion. For this we make use of in situ plasma and neutral gas measurements over the period 2015 August 1 to September 15 (roughly half a month pre- to a month post-perihelion). The free-electron number densities, n_e, shown in Figure 2(a) are taken from a recently released cross-calibrated data set (cf. Johansson et al. 2021) combining measurements by the MIP and the dual LAP, both being instruments within the Rosetta Plasma Consortium (RPC; Carr et al. 2007). The neutral number densities (scaled down by a factor of 10^{-6} in Fig 2(a)) are from measurements by ROSINA/COPS, corrected for background and assumption of H_2O dominance (Gasc et al. 2017), and we have excluded data associated with official wheel offloading periods and times when the off-pointing (off-nadir) angle exceeded 10°. The corresponding electron to neutral number density ratios are shown in Figure 2(b).

The median n_e/n_N ratio during the time interval is 4.06×10^{-5}. The "level of electron depletion" can be said to correspond to the ratio $(n_i - n_e)/n_i$, where n_i is the number density of positive ions. As we expect negatively charged grains, we have $n_i = n_e + n_{e,\mathrm{dust}}$

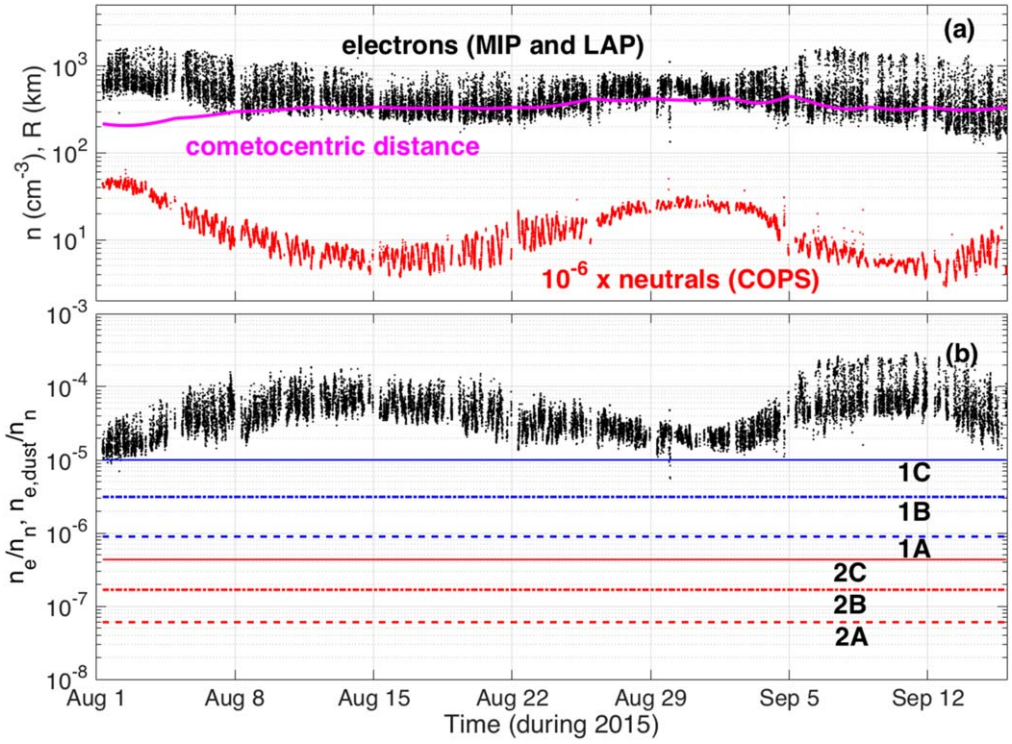

Figure 2. (a) Electron number density (black) measured by RPC/MIP and/or RPC/LAP and scaled-down neutral number density (red) measured by ROSINA/COPS, from 2015 Aug 1 to 2015 Sep 15 (including perihelion passage on Aug 15). The cometocentric distance, varying between 200 km and 449 km, is shown in magenta. (b) The electron to neutral number density ratio over the same time period. The horizontal lines represent the calculated $n_{e,\mathrm{dust}}/n_N$ ratios from the six considered parameter sets (see Tables 1 and 2).

and the level of electron depletion thus follows from

$$\text{Level of electron depletion} = \frac{n_{e,\mathrm{dust}}}{n_e + n_{e,\mathrm{dust}}} = \frac{n_{e,\mathrm{dust}}/n_N}{n_e/n_N + n_{e,\mathrm{dust}}/n_N}, \quad (4)$$

where the last step allows us to make direct use of the ratios listed in Table 2. We thereby find, when combined with the above given median n_e/n_N ratio, "typical quiescent" electron depletion levels as low as 0.1% (model with parameter set of Type 2A) up to ~20% (model with parameter set of Type 1C) as shown within brackets in Table 1. The parameter set 1C is the one invoking both the smaller "smallest dust size" and the steepest dust size distribution. This parameter set gives occasionally calculated depletion levels of 40–50%, but at this stage, it is worthwhile to remind readers about the lack of evidence of a ubiquitous presence of 10 nm grains (see Section 3.2).

Our data set pertains to 1 minute averages from the available COPS and LAP/MIP data, and we cannot completely rule out the existence of short-lasting events where the electron depletion from grain charging did reach significant levels. However, it is clear that a general/ubiquitous electron depletion is not supported by our model–observation comparisons.

Preliminary checks do not obviously tie reported major dust outbursts (e.g., Bockelée-Morvan et al. 2017; Rinaldi et al. 2018) to reductions in the electron-to-neutral number density ratios. For the time being we merely note that a (hypothetical) confirmation of no obvious reduction in n_e/n_N in response to Rosetta being situated in more dusty environments than usual (while near perihelion) potentially could be taken as an indication of a low level of electron depletion to start with. However, detailed event studies (akin to the study at lower activity by Hajra et al. 2017) is needed to enable more conclusive statements to be made on how outbursts affect the ionization balance near perihelion. Remote observations of outbursts (by, e.g., OSIRIS and VIRTIS) are typically done at ~90° when Rosetta is in the terminator plane. Hence, there is a time delay before such an outburst would cross Rosetta's path, which is a prerequisite for an in situ detection of the dust by, e.g., GIADA or the associated gas by ROSINA.

Our results should be viewed in light of the assumption that all grains have had time to actually acquire equilibrium charge, which is a more questionable assumption the smaller the grains under consideration. As discussed by, e.g., Cui & Goree (1994), the charging time, τ, is inversely proportional to the grain radius and the ambient plasma number density: $\tau = \mathrm{K}_\tau \sqrt{T_{\mathrm{eV}}}/(r n_e)$, where K_τ is a constant depending on the ion mass and the ratio of ion temperature to electron temperature. We note that K_τ increases with increasing ion mass and the closer to unity the ion-to-electron temperature ratio is set. The value of K_τ relevant to this study ought to be smaller than that given by Cui & Goree (1994) for an argon plasma with a unit ion-to-electron temperature ratio, $\mathrm{K}_\tau = 3.29 \times 10^3$ (unit of $\mathrm{m^2\,s\,eV^{-1/2}}$). From the measured electron number densities we take $n_e = 500\,\mathrm{cm^{-3}}$ as a typical ambient electron number density at Rosetta when near a cometocentric distance, R, of 300 km (see Figure 2(a)). Under the assumption of an isothermal plasma decaying as $1/R$ we may calculate from what distance R_* a grain of radius r and velocity u_D needs to start "charging up" in order for it to have reached equilibrium charge by the time it reaches the Rosetta cometocentric distance, R_{ROS}. This is approximated via the

criterion

$$\frac{rn_{e,\mathrm{ROS}}R_{\mathrm{ROS}}}{u_D K_\tau \sqrt{T_{\mathrm{eV}}}} \int_{R_*}^{R_{\mathrm{ROS}}} \frac{dR}{R} = \frac{rn_{e,\mathrm{ROS}}R_{\mathrm{ROS}}}{u_D K_\tau \sqrt{T_{\mathrm{eV}}}} \ln\left(\frac{R_{\mathrm{ROS}}}{R_*}\right) = 1, \quad (5)$$

where $n_{e,\mathrm{ROS}}$ is the electron number density at the location of Rosetta. For a grain in a plasma of constant density and temperature, the corresponding criterion would be $t_*\tau^{-1} = 1$ and then instead answer the question what time t_* an initially uncharged grain requires to charge up to the equilibrium value (then clearly, $t_* = \tau$). In Equation (5), dR/u_D corresponds to a time increment dt and the integral can be rewritten as one over time involving a time-dependent τ^{-1}. From Equation (5), using a conservative $K_\tau = 3.29 \times 10^3\ \mathrm{m^2\ s/eV^{1/2}}$, $T_{\mathrm{eV}} = 2.7$ eV, $R_{\mathrm{ROS}} =$ 300 km, $n_{e,\mathrm{ROS}} = 500\ \mathrm{cm^{-3}}$, and u_D depending on r according to $u_d(r) = c_2 r^{-\beta}$ with $c_2 = 0.2349\ \mathrm{m^{\beta+1} s^{-1}}$ and $\beta = 0.4272$ (see Section 3.4), we find as examples R_* values of ~33 km, ~276 km, and ~299 km for grains with radii of 10 nm, 100 nm, and 1000 nm, respectively. The assumption that the grains have an equilibrium charge does seem reasonable at least for grains with radii of several tens of nanometers or larger. For grains as small as 10 nm, the above analysis does not really provide a conclusive answer as to whether equilibrium charge safely can be assumed, mainly because it is questionable whether the underlying simplifying assumption of constant electron temperature used in Equation (5) applies, say for cometocentric distances <100 km. The possibility remains that grains as small as 10 nm in radius (parameter sets 1A, 1B, and 1C) may not have acquired equilibrium charge by the time they reach Rosetta, if anything (modestly) strengthening our claim of a typically rather low level of electron depletion.

4.2. Effect of the Negative Spacecraft Potential

With a spacecraft potential of $U_{\mathrm{SC}} \approx -15$ V (e.g., Odelstad et al. 2015, 2017), negatively charged grains need a certain minimum kinetic energy E_{min} in order to be able to reach onboard instrumentation (e.g., GIADA and MIDAS). The potential barrier (in joule) amounts to $U_{\mathrm{SC}}Q_r$, where Q_r is the charge of a grain of radius r. From Section 2 we notice that

$$Q_r = 4\pi\varepsilon_0\kappa_e U_D r, \quad (6)$$

so that

$$E_{\mathrm{min}}(r) = 4\pi\varepsilon_0\kappa_e U_D U_{\mathrm{SC}} r. \quad (7)$$

The kinetic energy (in joule) of a dust grain with radius r, mass density ρ, and velocity u_D is given by

$$E_{\mathrm{kin}}(r) = \frac{1}{2}\left(\frac{4}{3}\pi r^3\right)\rho u_D^2. \quad (8)$$

By equating Equations (7) and (8), it follows that the minimum velocity required for a dust particle to reach the (repelling) spacecraft is given by

$$u_{d,\mathrm{min}}(r) = \frac{1}{r}\sqrt{\frac{6\varepsilon_0\kappa_e U_D U_{\mathrm{SC}}}{\rho}}. \quad (9)$$

The dashed magenta line in Figure 1 shows against grain radius the minimum velocity needed to overcome a spacecraft potential of −15 V (we have assumed a grain potential of −10 V, a dielectric constant of 2, and a grain mass density of 533 kg m^{-3}). It can be seen that for sizes of several tens of nanometers and larger, the anticipated dust velocities (from the work of Marschall et al. 2020) are markedly higher than the minimum velocities needed. This favors that dust size distributions inferred from onboard instrumentation to first order should not have been severely skewed by the presence of the potential field around the spacecraft. This is consistent with the analysis of Fulle et al. (2015), who conclude that the dynamics of compact particles of sizes $>10^{-5}$ m are not affected by the spacecraft potential. Fulle et al. (2016) show that extremely fluffy grains (densities of the order of 1 kg m^{-3}) may undergo fragmentation when approaching a highly charged spacecraft. Dust fragmentation at a distance from the nucleus could potentially render small and slow-moving dust particles incapable of reaching onboard instrumentation. Also, by guidance of Figure 1, it appears that IES detection of grains in the nanometer size regime may have been prohibited by the spacecraft potential. This may complicate attempts to confirm "our case" via examination of IES data acquired near perihelion.

5. Summary and Concluding Remarks

We have presented an analytical model for calculating the number density of electrons attached to dust particles, $n_{e,\mathrm{dust}}$, in the coma of 67P. Central simplifying aspects include, but are not limited to, the assumption (i) of spherical dust particles moving radially outwards without undergoing fragmentation, (ii) that the dust size distribution obeys a single power-law relation, and (iii) that the dust grains, regardless of size, are charged to an equilibrium value approximated as the product of the capacitance (proportional to radius) and potential (assumed constant and independent of e.g., the ambient plasma and neutral number density). In addition to these simplifying assumptions, it is stressed that the resulting Equation (3) includes several parameters that are not tightly constrained. By considering the sets of parameters presented in Table 1 (and discussed in Section 3) in combination with electron and neutral number densities from in situ measurements near perihelion, we arrived in Section 4.1 (Table 2) at quiescent electron depletion levels between ~0.1% and ~20%. The higher level comes from a parameter set in which the single-exponent dust size distribution extends all the way down to 10 nm grains, the ubiquitous presence of which lacks any evidence. Moreover, it can be argued that the right-hand side of Equation (3) in a sense represents an upper limit of $n_{e,\mathrm{dust}}$ as we assume all grains to have acquired equilibrium charge and as we do not take into consideration the fact that in a dusty plasma there may not be sufficient numbers of free electrons around to charge up all grains to the equilibrium potential. Combined, we suggest that the typical level of electron depletion (near the Rosetta position) probably was less than 10% and possibly less than 1%.

Our proposed results are in stark contrast with Cassini's results from the water-dominated plumes of Enceladus where the level of electron depletion reportedly exceeds 90% in regions (Morooka et al. 2011). This is intriguing considering some comet-like attributes of Enceladus (e.g., Boice & Goldstein 2010). Enceladus is obviously much farther away

from the Sun than 67P is close to its perihelion. The resulting reduced photoionization rate may be a contributing factor to the higher level of electron depletion at Enceladus. However, we believe a more important discriminating aspect concerns the properties and formation processes of the dust particles in the respective environments. At Enceladus, the formation and processing of ice/dust particles are ongoing, occurring from liquid water expanding as jets through cracks in the ice cover (Porco et al. 2006; Hsu et al. 2015). This involves the formation and ejection of particles down to very small sizes as is evident from the detection of charged particles in the nanometer size regime (Hill et al. 2012). The situation at comets is quite different. Micrometer-sized (and larger) dust aggregates at 67P bear resemblance with interplanetary dust particles, indicating that the latter could represent a fraction of the building blocks of comets (e.g., Bentley et al. 2016; Langevin et al. 2016). Sufficiently close to the Sun, these large grains are released as the volatile part of the solid material on the surface (and in near-surface layers) sublimates due to solar heating. The grains leave the surface mainly under the influence of a gentle gas pressure gradient, sufficient to lift the grains but not to rapidly fragment them into the tens to hundreds of nanometer-sized parts they have been suggested to composed of (Bentley et al. 2016; Mannel et al. 2016, 2019; Güttler et al. 2019).

As noted in Section 1, a fast flyby investigation (Cassini) makes it easier to identify in Langmuir probe sweep analysis discrepancies between number densities of electrons and positive ions (a direct consequence of grain charging). It may be that future fast flyby missions at comets (like Comet Interceptor; see, e.g., Snodgrass & Jones 2019) can shed more light on the question of electron depletion in cometary comae. Meanwhile, the rich data set from Rosetta remains to be further explored. For instance, a careful examination of IES spectra acquired while Rosetta was close to perihelion may set constraints on the abundance of charged grains. We are not aware of any such study proposing the prevalent presence of charged nanodust, but at the same time, we have not seen works explicitly suggesting the opposite. From a modeling point of view, numerical simulations can be useful to relax some of the simplifying assumptions needed for the present analytical model. For example, particles of different sizes and charge states respond differently to gas pressure gradients and the electromagnetic field environment, thus rendering a size-dependent expansion cone. It is our hope that innovative ideas and associated detailed studies will enable more firm conclusions to be drawn to either support or rebuke our current view of a typically rather limited influence of dust on the ionization balance in the inner coma of 67P. From the present work, a significant level of electron depletion seems to require the dust size distribution to extend to sizes much below the 50–500 nm range proposed to be the smallest solid particle size by Güttler et al. (2019).

Rosetta is an ESA mission with contributions from its member states and NASA. F.L.J. acknowledges support from the Swedish National Space Agency under grant Dnr 168/15. The cross-calibration of LAP and MIP data was supported by ESA as part of the Rosetta Extended Archive activities, under contract 4000118957/16/ES/JD. R.M. and M.R. acknowledge the support from the Swiss National Science Foundation grants 184482 and 182418, respectively. We thank anonymous reviewers for helping to improve the quality of our manuscript.

ORCID iDs

E. Vigren https://orcid.org/0000-0003-2647-8259
A. I. Eriksson https://orcid.org/0000-0003-2926-6761
F. L. Johansson https://orcid.org/0000-0002-5386-8255
R. Marschall https://orcid.org/0000-0002-0362-0403
M. Morooka https://orcid.org/0000-0001-9958-0241
M. Rubin https://orcid.org/0000-0001-6549-3318

References

Balsiger, H., Altwegg, K., Bochsler, P., et al. 2007, SSRv, 128, 745
Bentley, M. S., Schmied, R., Mannel, T., et al. 2016, Natur, 537, 73
Biver, N., Bockelée-Morvan, D., Hofstadter, M., et al. 2019, A&A, 630, A19
Bockelée-Morvan, D., Rinaldi, G., Erard, S., et al. 2017, MNRAS, 469, S443
Boehnhardt, H., Riffeser, A., Kluge, M., et al. 2016, MNRAS, 462, S376
Boice, D. C., & Goldstein, R. 2010, in Proc. IAU Symp. 263, Icy Bodies of the Solar System, ed. J. A. Fernández et al. (Cambridge: Cambridge Univ. Press), 151
Burch, J. L., Goldstein, R., Cravens, T. E., et al. 2007, SSRv, 128, 697
Burch, J. L., Gombosi, T. I., Clark, G., et al. 2015, GRL, 42, 6575
Carr, C., Cupido, E., Lee, C. G. Y., et al. 2007, SSRv, 128, 629
Coates, A. J., Crary, F. J., Lewis, G. R., et al. 2007, GRL, 34, L22103
Cui, C., & Goree, J. 1994, ITPS, 22, 151
Davidsson, B. J. R., Gulkis, S., Alexander, C., et al. 2010, Icar, 210, 455
Draine, B. T., & Sutin, B. 1987, ApJ, 320, 803
Engelhardt, I. A., Eriksson, A. I., Vigren, E., et al. 2018, A&A, 616, A51
Eriksson, A. I., Boström, R., Gill, R., et al. 2007, SSRv, 128, 729
Eriksson, A. I., Engelhardt, I. A., André, M., et al. 2017, A&A, 605, A14
Fulle, M., Della Corte, V., Rotundi, A., et al. 2015, ApJL, 802, L12
Fulle, M., Marzari, F., Della Corte, V., et al. 2016, ApJ, 821, 19
Gasc, S., Altwegg, K., Fiethe, B., et al. 2017, P&SS, 135, 64
Gilet, N., Henri, P., Wattieaux, G., et al. 2020, A&A, 640, A110
Gombosi, T. I., Burch, J. L., & Horányi, M. 2015, A&A, 583, A23
Goree, J. 1994, PSST, 3, 40
Güttler, C., Mannel, T., Rotundi, A., et al. 2019, A&A, 630, A24
Hajra, R., Henri, P., Vallières, X., et al. 2017, A&A, 607, A34
Hansen, K. C., Altwegg, K., Berthelier, J.-J., et al. 2016, MNRAS, 462, S491
Herique, A., Kofman, W., Beck, P., et al. 2016, MNRAS, 462, S516
Hill, T. W., Thomsen, M. F., Tokar, R. L., et al. 2012, JGR, 117, A05209
Hornung, K., Merouane, S., Hilchenbach, M., et al. 2016, P&SS, 133, 63
Hsu, H.-W., Postberg, F., Sekine, Y., et al. 2015, Natur, 519, 207
Johansson, F. L., Eriksson, A. I., Vigren, E., et al. 2021, A&A, in press
Johansson, F. L., Odelstad, E., Paulsson, J. J. P., et al. 2017, MNRAS, 469, S626
Keller, H. U., Barbieri, C., Lamy, P., et al. 2007, SSRv, 128, 433
Langevin, Y., Hilchenbach, M., Ligier, N., et al. 2016, Icar., 271, 76
Larsen, T. R., Jespersen, M., Murdin, J., et al. 1972, JATP, 34, 787
Lavvas, P., Yelle, R. V., Koskinen, T., et al. 2013, PNAS, 110, 2729
Llera, K., Burch, J. L., Goldstein, R., & Goetz, C. 2020, GRL, 47, e86147
Mannel, T., Bentley, M. S., Boakes, P. D., et al. 2019, A&A, 630, A26
Mannel, T., Bentley, M. S., Schmied, R., et al. 2016, MNRAS, 462, S304
Marschall, R., Markkanen, J., Gerig, S.-B., et al. 2020, FrP, 8, 227
Mendis, D. A., & Horányi, M. 2013, RvGeo, 51, 53
Merouane, S., Stenzel, O., Hilchenbach, M., et al. 2017, MNRAS, 469, S459
Meyer-Vernet, N. 2013, Icar, 226, 583
Moreno, F., Muñoz, O., Gutiérrez, P. J., et al. 2017, MNRAS, 469, S186
Morooka, M. W., Wahlund, J.-E., Eriksson, A. I., et al. 2011, JGR, 116, A12221
Morooka, M. W., Wahlund, J.-E., Hadid, L. Z., et al. 2019, JGRA, 124, 1679
Notni, P., & Tiersch, H. 1987, A&A, 187, 796
Odelstad, E., Eriksson, A. E., Johansson, F. L., et al. 2018, JGRA, 123, 5870
Odelstad, E., Eriksson, A. I., Edberg, N. J. T., et al. 2015, GRL, 42, 10126
Odelstad, E., Stenberg Wieser, G., Wieser, M., et al. 2017, MNRAS, 469, S568
Ott, T., Drolshagen, E., Koschny, D., et al. 2017, MNRAS, 469, S276
Pätzold, M., Andert, T., Hahn, M., et al. 2016, Natur, 530, 63
Pätzold, M., Andert, T. P., Hahn, M., et al. 2019, MNRAS, 483, 2337

Porco, C. C., Helfenstein, P., Thomas, P. C., et al. 2006, Sci., 311, 1393
Rinaldi, G., Bockelée-Morvan, D., Ciarnello, M., et al. 2018, MNRAS, 481, 1235
Rotundi, A., Sierks, H., Della Corte, V., et al. 2015, Sci., 347, aaa3905
Shebanits, O., Wahlund, J.-E., Mandt, K., et al. 2013, P&SS, 84, 153
Snodgrass, C., & Jones, G. H. 2019, NatCo, 10, 5418
Snodgrass, C., Tubiana, C., Bramich, D. M., et al. 2013, A&A, 557, A33
Tenishev, V., Combi, M. R., & Rubin, M. 2011, ApJ, 732, 104
Vigren, E., Edberg, N. J. T., Eriksson, A. I., et al. 2019, ApJ, 881, 6
Vigren, E., Galand, M., Eriksson, A. I., et al. 2015, ApJ, 798, 130